Trans Indian Inst Met (2014) 67(2):247–262
DOI 10.1007/s12666-013-0344-9

TECHNICAL PAPER

TP 2755

Effect of N_2 and He Carrier Gases on Oxidation Behavior of Cold Sprayed CoNiCrAlY Powder to Deposit Bond Coats

W. S. Rathod · A. S. Khanna · J. Karthikeyan · R. C. Rathod

Received: 24 December 2012 / Accepted: 1 July 2013 / Published online: 10 October 2013

Abstract CoNiCrAlY has been cold sprayed onto 316L substrate using helium and nitrogen as carrier gases. CGDS with helium gas under the temperature of 400 °C and pressure of 20 bars and CGDS with nitrogen gas under the temperature of 450 °C and pressure of 38 bars were used. The purpose of the current study was to investigate the microstructure and oxidation behavior of CoNiCrAlY coatings deposited by CGDS technique with both carrier gases. The quality of the as-sprayed and oxidized bond coats was assessed and investigated from the point of view of microstructural (porosity and oxide concentration) and mechanical properties (hardness) characteristics. Sprayed samples were exposed to isothermal oxidation at 900 °C in air. Oxide growth rates were obtained from a series of mass gain measurement while oxide scale compositions were determined using SEM, XRD and EDX analysis. Helium processing condition displays more compact structure for the coating when compared to N_2. The oxide scale on the CGDS sprayed with He coating after 1,000 h of oxidation is composed of alumina without the presence of detrimental fast growing mixed oxides. Results obtained in this study show that CGDS sprayed with N_2 coating features high levels of visible defects, oxide content, spinal-type oxide and high oxide growth rate, whereas CGDS with He shows low oxide growth rate due to low porosity and oxide content.

W. S. Rathod (✉) · A. S. Khanna
Corrosion Science & Engineering Department, IIT Bombay, Mumbai, India
e-mail: wsrathod@vjti.org.in

J. Karthikeyan
ASB Industries, Barberton, OH, USA

R. C. Rathod
Metallurgy Department, VNIT, Nagpur, India

Keywords Cold gas dynamic spray (CGDS) · Oxidation · Bond coat · Spinal · Porosity

1 Introduction

In CGDS technique, the kinetic energy, rather than thermal energy is used to produce the bond coat [1, 2]. In this process, the fine powders particles (5–42 μm diameter) are propelled in a supersonic flow and get deposited on substrate after undergoing sever plastic deformation upon impacting the substrate. CGDS coating operates at lower temperatures and also uses inert gases such as helium and nitrogen which hinder oxidation and grain growth during deposition [3–7].

Analysis of the detailed microstructure of the coating does not show any evidence of the melting of the spray powder particles. The high velocity is developed by He and N_2 carrier gases through high inlet pressure in a converging and diverging de Laval type of nozzle [7]. With increasing velocities, the powder particles undergo by process of erosion and abrasion deposition onto substrate. Higher impact velocities develop high-plastic deformations, yielding better binding between particles and substrate, leading to lower porosities. Hence, critical velocity is a definite requirement for generating sufficient kinetic energy to cause plastic deformation of the surfaces. CGDS process with He carrier gas, depicts heavy plastic deformation and dense coating. This effect is due to low carrier gas density, higher specific heat ratio, and lower molecular weight which results in higher kinetic energy; whereas CGDS processed with N_2 carrier gas display relatively higher degree of porosity. This behavior is due to the increase in density of the carrier gas and thereby reduced kinetic energy and degree of plastic deformation of the spray particles [8, 9].

Richer et al. [10, 11] deposited CoNiCrAlY coating using CGDS sprayed with He gas reported that coating composed of alumina, without the presence of NiO or spinal-type mixed oxides.

Zhang et al. [12] studied oxidation behavior of NiCrAlY using CGDS technique. They found at 900 °C and 1,000 °C only alumina (α-A_2O_3) in the oxide scales. Tang et al. [13] deposited CoNiCrAlY coating by HVOF and reported that in-process surface oxidation is detrimental to the TGO growth mechanism, as it promotes the onset undesirable fast-growing nonaluminum oxides that form protrusions and results in the TBC failure.

The aim of the present work was to compare the oxidation behavior of the bond coat material applied using two CGDS technique, sprayed with He and N_2 carrier gases. The difference in coating characteristics is expected due to the large difference in the density, specific heat ratio, and molecular weight of the carrier gases which in turn can modify the oxidation behavior of the coatings.

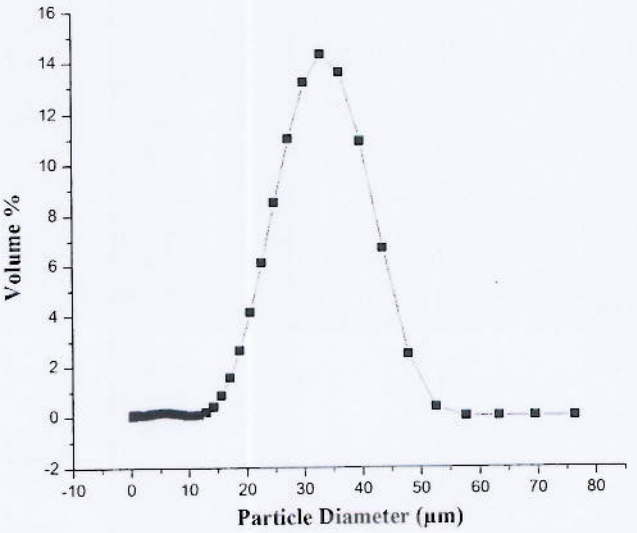

Fig. 1 Plot of cumulative vol% particle diameter for the as-received CoNiCrAlY powder

2 Experimental Procedure

2.1 Feedstock Powder

The feedstock material chosen in this study is a commercially available CoNiCrAlY alloy, purchased from M/s. Metallizing Equipment Pvt. Ltd. Jodhpur, trade name MEC 9950 AMF powder with a nominal composition of CoNiCrAlY. The detail of the powder used to carry out the work is shown in Table 1. Figure 1 illustrates the cumulative result obtained from particle size analyzer (Laser Diffraction LS 13320) for powder. The distribution of particles size is homogenous with an average of approximately 32 μm.

2.2 CoNiCrAlY Powder Characterization

Figure 2 shows XRD pattern of CoNiCrAlY powder, surface morphology and EDX analysis of elemental composition (wt%) at selected points. This gas atomized powder has a spherical morphology and particle size range (10–42 μm diameter). Furthermore, the EDX spectrum of the powder particles is taken in order to confirm the composition given by suppliers. The observed composition of the material to that submitted by supplier is in considerable agreement, except for a small concentration of yttrium. Figure 3 shows the cross-section of the powder particles and EDX analysis at selected points. Since the γ phase is a solid solution of Co, Ni, Cr etc. and has a higher mean atomic number, it appears brighter in BSE mode. Hence, the brighter phase is considered to be γ. The darker phase which has a lower mean atomic number in BSE mode is considered to be β-NiAl/CoAl intermetallic. These phases are also confirmed from XRD pattern (Fig. 2) [11–13]. Comparing the elemental composition of the both phases, the values presented are an average of five different EDX measurements. The analysis reveals that the darker phase is enriched in Al, whereas the brighter phase is enriched in Cr. The γ phase is the major phase with β regions embedded.

3 Coating Deposition by CGDS Sprayed with He and N_2 Coatings

Cold spraying of fine, spherical CoNiCrAlY powder, as shown in Fig. 2, in the size range of 10–42 μm was done with supersonic velocity onto 316L substrate using a spray gun with converging–diverging nozzle at ASB Industries, Ohio. The schematic of the cold-spray process is shown in Fig. 4 [14]. The powder was fed through a high-pressure hopper, mixed with the preheated gas in a mixing chamber inside the gun, and was deposited at a very high pressure on to the substrate. In order to understand the effect of different specific-heat ratios in terms of coating performance, two

Table 1 Chemical composition of powder

Elements →	Co	Ni	Cr	Al	O	Y
Wt% →	38.25	32.33	20.51	8.90	00	0.01

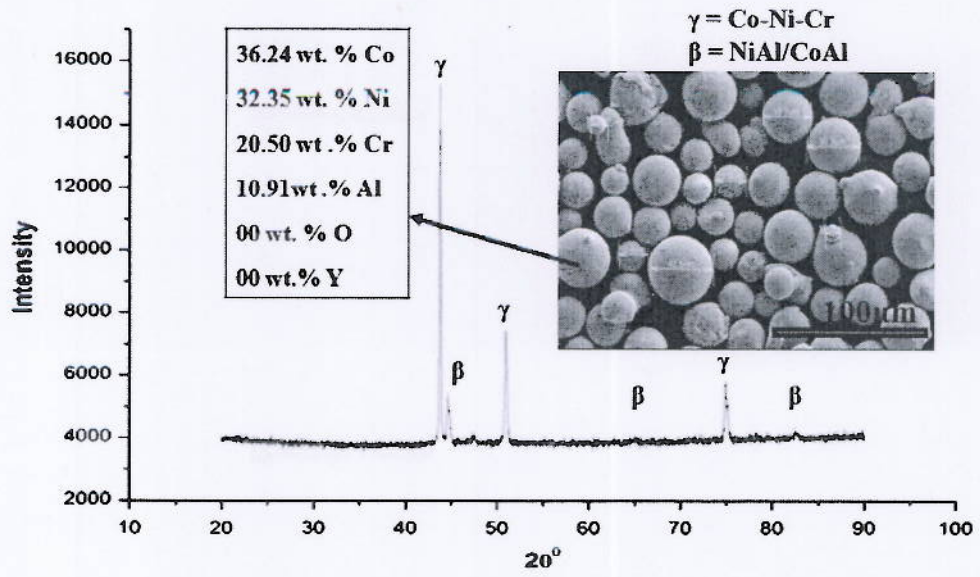

Fig. 2 XRD pattern of CoNiCrAlY powder revealing a two-phases, γ+β structure

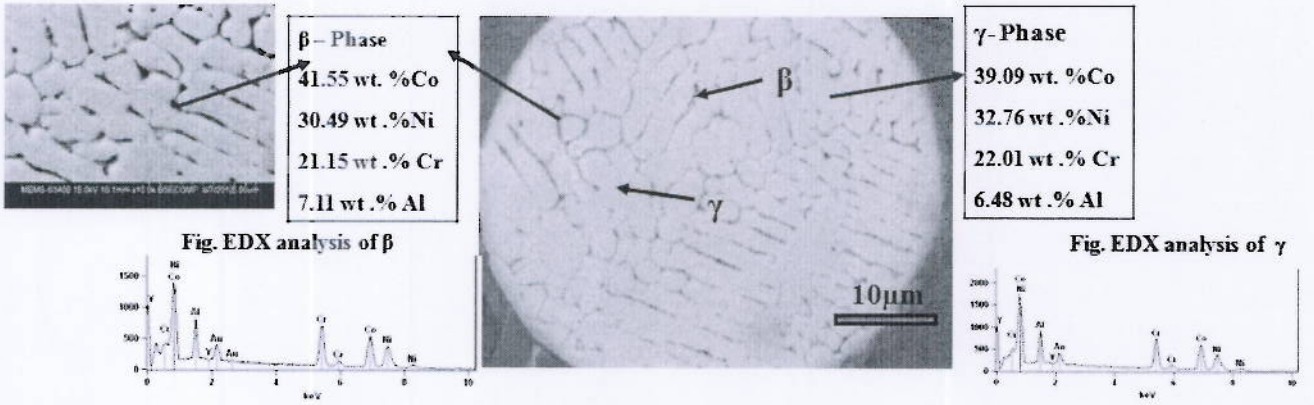

Fig. 3 SEM micrograph of CoNiCrAlY powder, illustrating atomic number contrast due to a two-phase structure

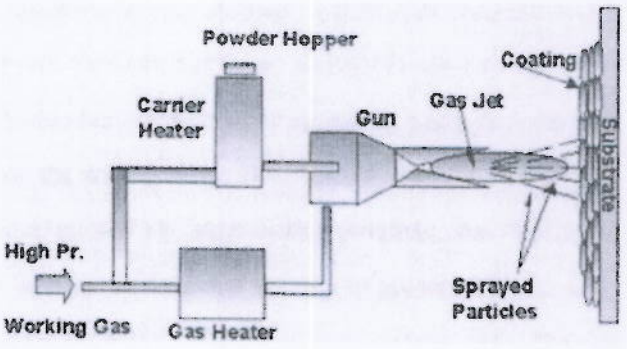

Fig. 4 Schematic of the cold spray system

different gas compositions, i.e., He and N_2, are employed to carry and accelerate the CoNiCrAlY powder.

The 316L stainless steel plates were cut into 300 × 300 × 2 mm size with a wheel cutter. Before deposition, the plates were grit blasted with 20-grit alumina at a pressure of 0.3 MPa to increase surface roughness and ultrasonically cleaned. The plates were then coated using Nitrogen and Helium gas with desired process parameters (Table 2). Finally plates were cut into small pieces of (10 × 10 × 2 mm) size using wire EDM for experiment. Surface morphology of as-deposited and oxidized samples were investigated qualitatively and quantitatively in order to assess their properties in the as-sprayed and oxidized condition using a SEM. Prior to microscopic investigations, the coated samples were sectioned and polished using standard metallographic techniques.

4 Results and Discussion

4.1 Surface Morphology and Microstructure of As-Sprayed CGDS Sprayed with He Coating

Figure 5 (a, b, c) shows the surface morphology, cross-sectional morphology and dendrites microstructure of as-

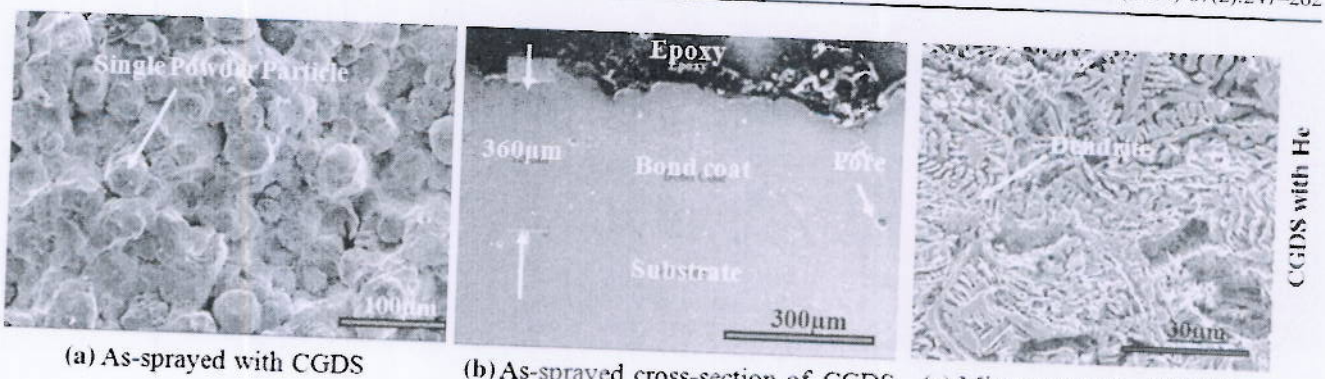

(a) As-sprayed with CGDS (b) As-sprayed cross-section of CGDS (c) Microstructure of CGDS

Fig. 5 SEM Images of CGDS coating sprayed with He gas in as-sprayed condition

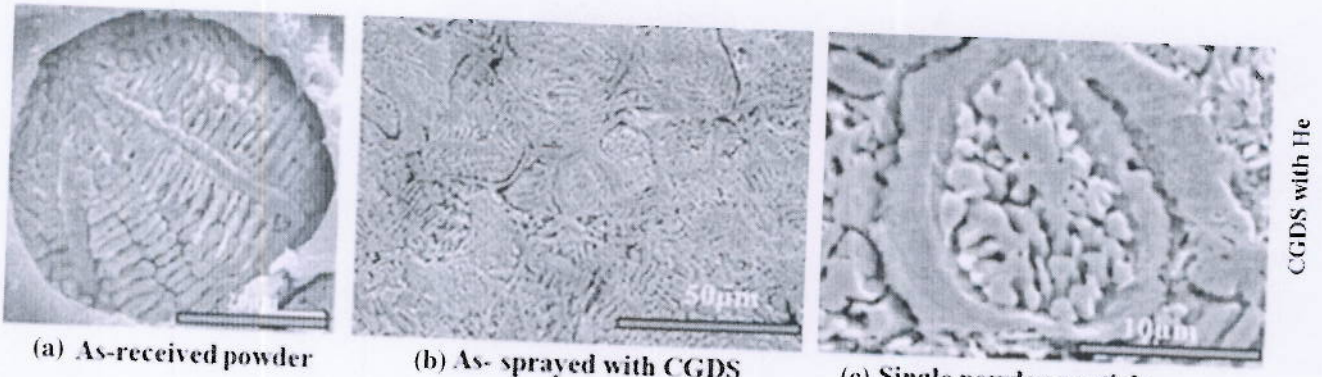

(a) As-received powder (b) As- sprayed with CGDS (c) Single powder particle

Fig. 6 **a** Secondary electron SEM images of etched cross section of powder revealing dendrite structure **b** as-sprayed CGDS cross-section revealing deformed dendrites **c** single powder particle in deformed condition

sprayed CGDS coating sprayed with He. The microstructure of CGDS with He clearly shows that CoNiCrAlY particles experience intensively plastic deformation during deposition. In cold spray, the powder is not molten before impacting on the substrate. It is generally accepted that mechanical bonding is the main mechanism of coating formation. The first layer of coating builds up when particles impact on the substrate. The deposition continues on the former layers. As a result, the increasing plastic deformation reduces the porosity of the former layers. The particle deformation enhances the squeeze among the particles so much that the voids disperse or minimize.

The SEM microstructure of the powder reveals solid state deposition particles present on the top of as-sprayed condition (Fig. 5a). Due to the deposition characteristics from the solid particles impact, a CGDS coating generally presents a high surface roughness. The coating surface is rough in the as-sprayed condition due to the presence of solid particles penned at surface partially deformed particles. From Fig. 5b, the thickness of the coating measured is in the range of 320–360 μm; while the cross-section of the CGDS coating shows a dense and uniform coating. The cold-sprayed CGDS coating, processed with He carrier gas composition, depicts heavy plastic deformation and reconsolidation into dense coating structures. Sonic velocity (v) in a media is given as $v = (\gamma RT/A)^{1/2}$, where γ is the specific heat ratio, R is universal gas constant, T is gas temperature, and A is molecular weight of the carrier gas. As helium is expected to provide tamping of the spray CoNiCrAlY powder onto substrate, due to low carrier gas density (0.1785 kg/m^3), higher specific heat ratio (1.660), lower molecular weight (4 g/mol) of helium and low density of CoNiCrAlY powder (7,824 kg/m^3), dense structure is endorsed in the SEM image (Fig. 6 b). Figure 6 (a, b, c) shows the as received powder cross-section, as-sprayed powder and single powder particle microstructure of CGDS coating sprayed with He.

The process of plastic deformation and reconsolidation of the impacting particles is distinct in this coating. It is very clear from Fig. 6 (b) to deduce the heavy impact of particles in Helium-processed coating with most of particles exceeding the critical velocity and getting deposited onto the substrate [1, 11, 14].

4.2 EDX Analysis of Upper Layer and Cross-Section of CGDS Coating Sprayed with Helium Gas

Figure 7 shows EDX analysis of surface and cross-section in as-sprayed condition. Coating sprayed with helium gas at upper layer and cross-section shows elemental composition (wt%) at selected points. Each value is an average of

Fig. 7 SEM images and EDX compositions of CGDS coating sprayed with He gas in as-sprayed condition

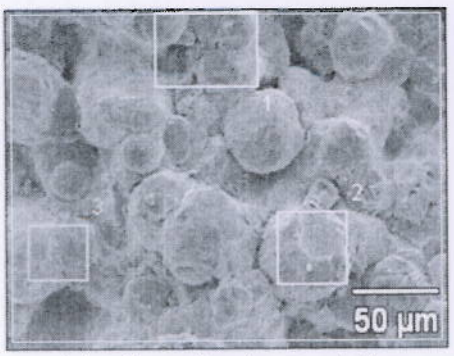

(a) As-Sprayed surface morphology

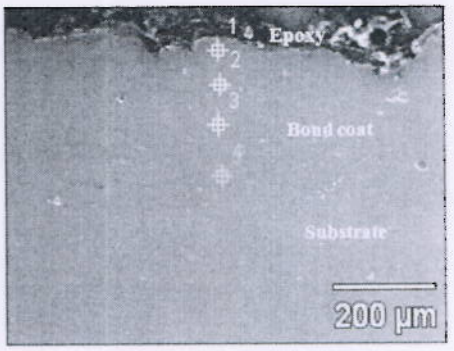

(b) As-Sprayed Cross-section

Table 1. EDX Analysis at areas

Point (Wt %) → Elements ↓	Average of three areas	Overall
Co	39.47	39.54
Ni	32.87	33.48
Cr	20.43	20.78
Al	6.53	5.63
O	0.67	0.56
Y	00	00

Table 2. EDX Analysis at points

Point (Wt %) → Elements ↓	1	2	3	4
Co	39.60	41.66	40.62	36.10
Ni	32.88	31.38	32.88	35.74
Cr	20.14	21.03	20.58	18.52
Al	6.61	5.44	5.77	8.99
O	0.77	0.49	0.14	0.65
Y	00	00	00	00

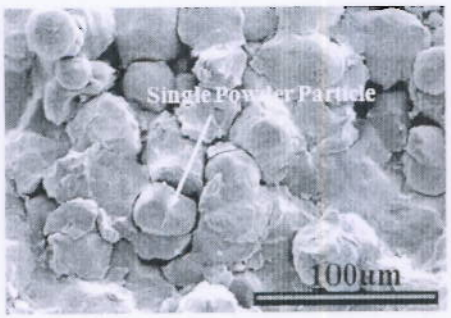

(a) As-sprayed with CGDS

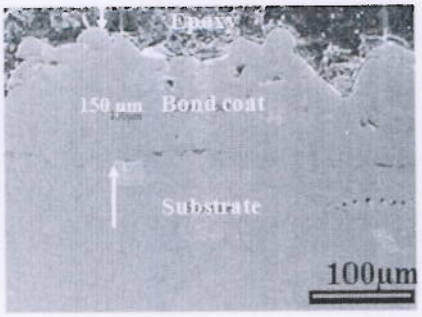

(b) As-sprayed cross-section of CGDS

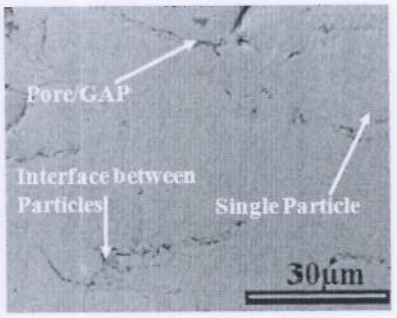

(c) Microstructure of CGDS

Fig. 8 SEM image of CGDS coating sprayed with N_2 gas in as-sprayed condition

at least 3 measurements. The EDAX analysis at some points indicates the dominance of Co and Ni and Cr in the composition of the coating as shown Fig. 7. This composition is nearly approaching the composition of the sprayed powder.

4.3 Surface Morphology and Microstructure of As-Sprayed CGDS Coating Sprayed with N_2 Gas

Figure 8 (a) indicates that the layer is impacted by particles that are not actually getting deposited (similar to shot blasting) because of not being able to acquire the critical velocity required for the deposition. Hence, multi-impacts under N_2 carrier gas display relatively higher degree of porosity, portraying low carrying capability of accelerating gas (Fig. 8b). This behavior is due to the increase in density of the carrier gas (N_2 density is 1.2506 kg/m^3), and thereby reduced degree of plastic deformation of the spray particles is expected for the coating. Moreover, higher porosity levels, larger splat size, and reduced plastic deformation degree are observed when compared to those of helium-processed coating.

Spray-coated micrograph (Fig. 8c) is to witness pores and voids of the N_2-processed coating structure. The presence of smaller splats in case of helium-processed coating is attributed to the higher degree of impact of the powders, whereas the spreader and higher splat size in N_2 processing is attributed to the multi-impacts on the coated layer. Figure 9 (a, b, c) shows the as received powder cross-section, as-sprayed powder and microstructure of CGDS coating sprayed with N_2. It is interesting to note that the dendrites microstructure of feedstock powder is also found on the as-sprayed sublayer of CGDS coating, consisting of interlocked dendrites, where most of the dendrites appear to be deformed significantly, giving a flattened appearance as compared to original dendrites of

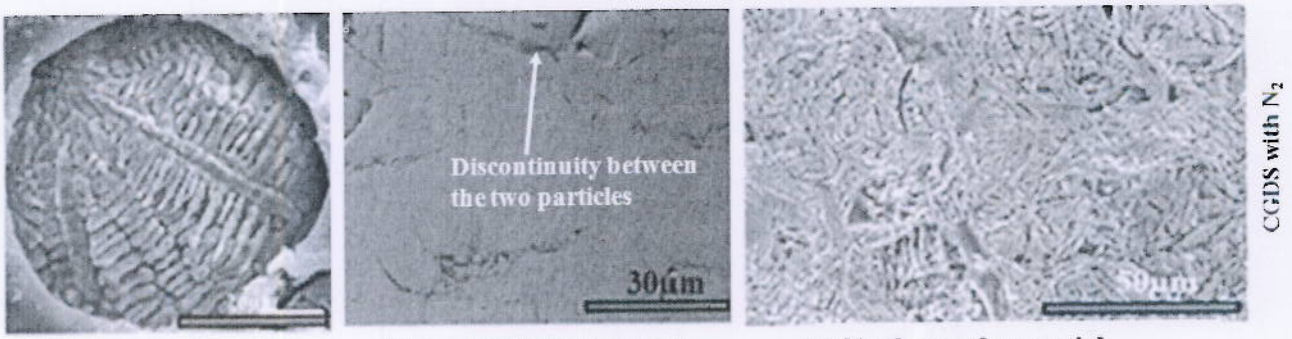

(a) As-sprayed powder (b) As-sprayed cross-section (c) Single powder particle

Fig. 9 **a** secondary electron SEM images of etched cross section of powder revealing dendritic structure **b** as-sprayed CGDS cross-section revealing deformed dendrites **c** single powder particle in deformed condition

Fig. 10 SEM images and EDX compositions of CGDS coating sprayed with N_2 gas in as-sprayed condition

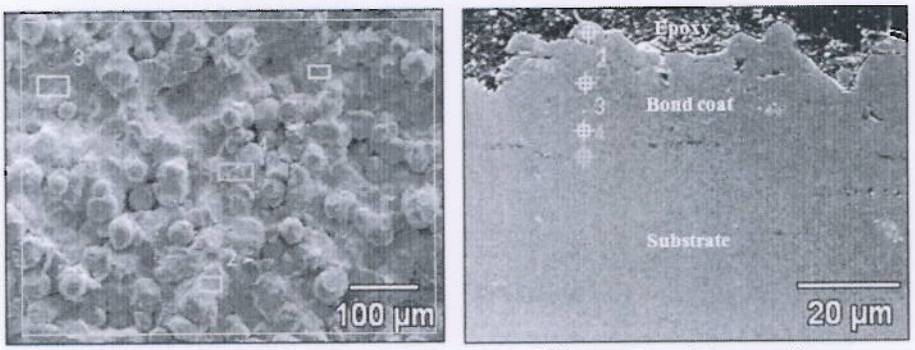

(a) As-Sprayed surface morphology (b) As-Sprayed Cross-section

Table 1. EDX Analysis at areas

Point (Wt %)→ Elements ↓	Average of four areas	Overall
Co	39.75	39.54
Ni	33.93	33.48
Cr	20.19	20.78
Al	5.95	5.63
O	0.14	0.56
Y	00	00

Table 2. EDX Analysis at points

Point (Wt %)→ Elements ↓	1	2	3	4
Co	38.28	38.22	36.52	33.74
Ni	33.35	32.88	33.58	26.65
Cr	19.67	20.38	20.34	19.38
Al	8.23	7.90	9.40	6.73
O	0.48	0.63	0.16	00
Y	00	00	00	00

the feedstock powder. To increase the particle velocity, thereby the kinetic energy of the spray particle, higher temperatures or lower molecular weight gases are required as accelerating gases.

4.4 EDX Analyses of Upper Layer and Cross-Section of As-Sprayed CGDS Coating Sprayed with N_2 Gas

Figure 10 shows EDX analyses of surface and cross-section in as-sprayed condition. Coating sprayed with nitrogen gas at upper layer and cross-section shows elemental composition (wt%) at selected points. Each value is an average of at least 4 measurements. The EDAX analysis at some points indicates the dominance of Co and Ni and Cr in the composition of the coating as shown in Fig. 10. This composition is nearly approaching the composition of the sprayed powder.

4.5 Properties of CGDS Coating Sprayed He and N_2 Gas

Figure 11 shows surface roughness and porosity measurement of CGDS sprayed with He and N_2 coatings. Surfaces roughness is measured for as-sprayed CGDS coating sprayed with He and N_2 coatings. Image analysis software is used for porosity measurement on cross-section of as-sprayed CGDS coating sprayed with He and N_2 coating. The CGDS both coatings show roughness value and porosity as shown in Table 3.

4.6 Nanoindentation Analysis of the Coatings

One of the latest methods of assessing the hardness of thin coated layer by nanoindentation. Figure 12 (a, b) shows the nanoindentation graph of CGDS sprayed with He and N_2 coatings. The load 11,000 g applied for 15 s. Six indents were made on each sample and averages of the results were

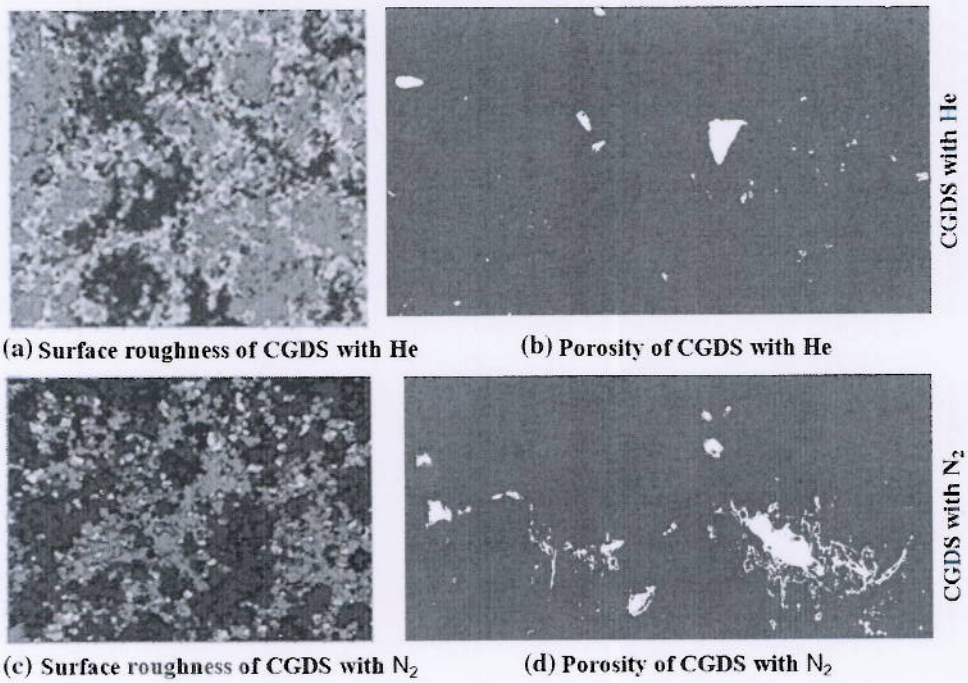

Fig. 11 Images of surface roughness and porosity measurement of CGDS sprayed with He and N_2 coatings

Table 2 Cold spray process parameter sprayed with Helium and N_2 gases

Parameter	He processing Values	N_2 processing Values
Gun temperature	400 °C	450 °C
Gun pressure	20 bars	38 bars
Powder feed rate	18 g/min	15 g/min
Carrier gas flow rate	3.0 m^3/hr	3.0 m^3/hr

taken. As observed in SEM micrographs, Fig. 5 (b) CGDS sprayed with He coating is very dense, as compared to the CGDS sprayed N_2 (Fig 8b). Helium (He) and nitrogen (N_2) processed deposition reveals same hardness values along cross-section, as quoted in Table 3 [15]. The coatings for both spraying conditions possess a higher hardness than substrate, providing sufficient protection to the substrate against wear and surface damages Table 4.

4.7 Isothermal Oxidation of Coatings at 900 °C for 1,000 h

4.7.1 Kinetics of CGDS Sprayed with He and N_2 Coatings

The oxidation kinetics is investigated using thrermogravimetrically. The weight changes of coatings were monitored during the isothermal oxidation in air for 1,000 h at 900 °C. Figure 13 shows the overall weight change of coatings sprayed with CGDS sprayed with He and N_2 gases as a function of time. The results show that the CGDS sprayed with He coated sample shows significant lower oxidation rate than the CGDS sprayed with N_2 coated samples. The linear plots appear to follow parabolic kinetics. The parabolic rate constants are determined using the equation. For evaluation, it is assumed that the oxidation follows a parabolic kinetic equation.

$$\left(\frac{\Delta m}{A}\right)^2 = K_p t$$

where Δm mass gain in g; A total surface area of the sample in cm^2; K_p constant in $g^2/cm^4\ s^{-1}$; t time in s.

The oxidation kinetics appears parabolic all along the oxidation test. After 1,000 h, the parabolic rate constant, K_p calculated using parabolic equation is found to be 0.510×10^{-8} $g^2/cm^4\ s^{-1}$; for N_2 gas and 0.100×10^{-8} $g^2/cm^4\ s^{-1}$ for He gas sprayed with CGDS [11, 13, 16]. The lower oxidation rate of the CGDS sprayed with He samples compared to that of N_2 samples can be attributed to the quick formation of α-Al_2O_3 layer during oxidation. This may be attributed to the immediate availability of enough aluminum on the surface, due to non diffusion of aluminum in the matrix, compared to CGDS sprayed with N_2 process, where part of aluminum diffuses into the matrix due to high temperature involved during coating. This appears to be a most important advantage of CGDS-He process over the CGDS-N_2 process. Coatings with low porosity and low oxide content exhibit the lowest oxide growth rates.

4.7.2 Oxidation of As-Sprayed Coatings

The protection offered by the alloy bond coat against high-temperature oxidation relies on the ability of the alloy to

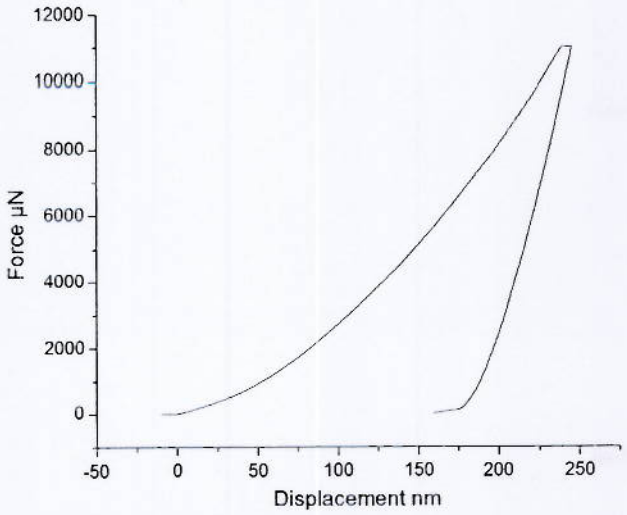

(a) Nanoindentation Graphs of CGDS Sprayed with He

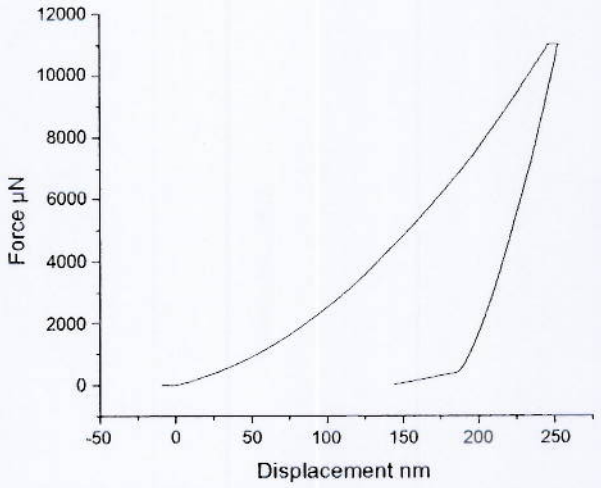

(b) Nanoindentation Graphs of CGDS Sprayed with N_2

Fig. 12 **a** Nanoindentation graphs of CGDS sprayed with He **b** nanoindentation graphs of CGDS sprayed with N_2

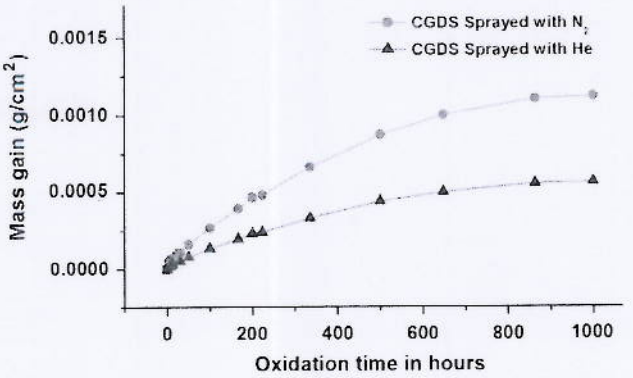

Fig. 13 Mass gain curve obtained during isothermal oxidation of the CGDS sprayed with He and N_2 coatings after the oxidation at 900 °C for 1,000 h

produce and maintain a stable, continuous, slow-growing and adherent oxide scale on its surface. The requirements are met best by a continuous α-Al_2O_3 scale, because the effective diffusion rates of oxygen and metal ions through α-Al_2O_3 are relatively low and the chemical and thermal stability of alumina is relatively high. Ideally, formation of an oxide scale constituted of α-Al_2O_3 during the entire period of oxidation is preferred. Therefore, to sustain the exclusive growth of α-Al_2O_3 on a CoNiCrAlY alloys at the onset of oxidation, the Al activity in the bond coat the oxide/metal interface has to remain high enough during oxidation to undergo rapid growth to form a continuous alumina scale on the bond coat surface.

4.8 Characterization of Oxide Scale Morphology, EDX and XRD Analysis of CGDS Coating Sprayed with He Gas Samples Exposed at 900 °C for Different Times

Figure 14 illustrates surface morphology of CGDS coating oxidized at 900 °C for 200, 500 and 1,000 h for isothermal

Table 3 Properties of He and N_2 processed CoNiCrAlY sprayed deposition

Deposition properties	He processing	N_2 processing
Thickness of coating	320–360 μm	105–115 μm
Microstructural features	Dense and compact coating	Pores and porosity
Surfaces roughness values Ra (μm)	23.41 ± 1.30	16.04 ± 1
Porosity level (%)	0.9 ± 0.8	5 ± 0.9
Extent of plastic deformation of powder particles	Insufficient plastic deformation	Lower degree of plastic deformation

Table 4 Nanoindentation of CGDS sprayed with He and N_2 in as-sprayed condition

Process	Load P_{max} (mN)	Hardness (GPa)	Reduced modules Er (GPa)	Depth of penetration H_{max} (nm)
CGDS He	11,000	6.61	153.38	245
CGDS N_2	11,000	6.26	145.04	253

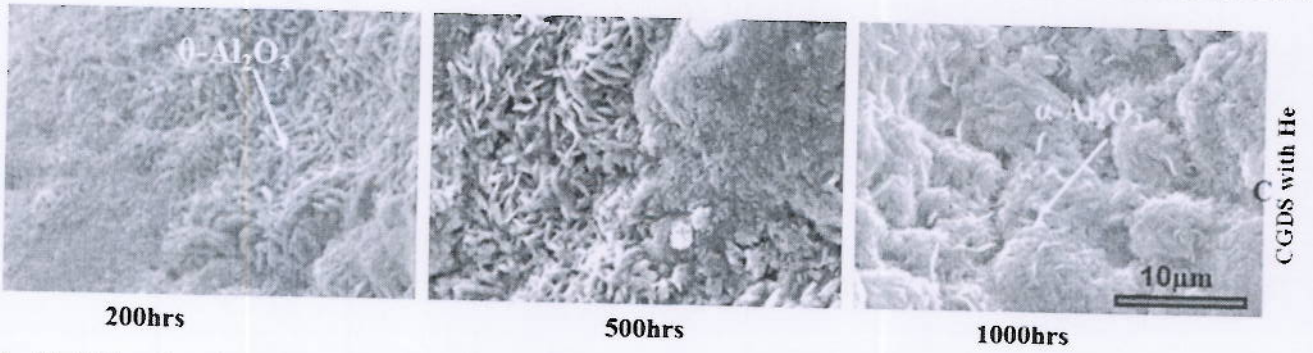

Fig. 14 Oxide scale surface morphology of the CGDS coating sprayed with He gas after the oxidation at 900 °C for different times

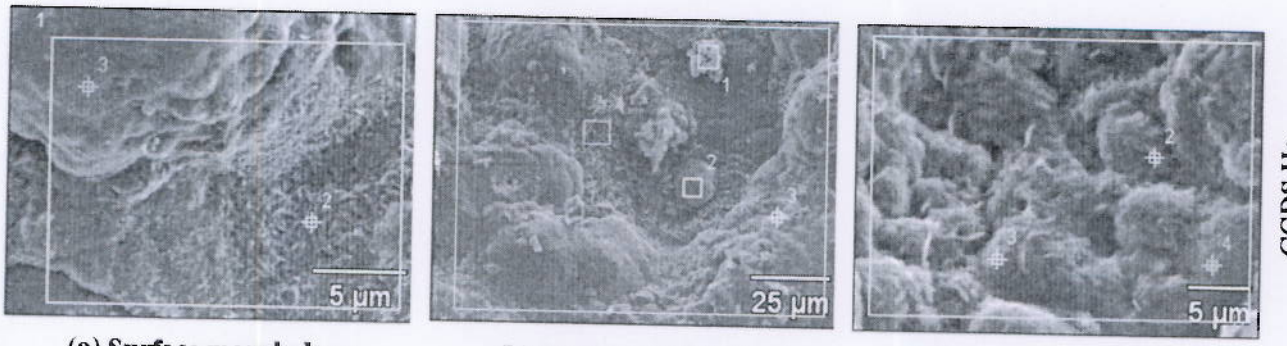

Table 1. EDX Analysis at points

Point (Wt%)→ Elements ↓	Overall	Averages of two points
Co	5.91	6.81
Ni	2.17	3.05
Cr	2.96	3.84
Al	52.97	54.18
O	35.98	32.10
Y	00	00

200 hrs

Table 2. EDX Analysis at points

Point (Wt%)→ Elements ↓	Overall	Averages of three points
Co	13.33	10.55
Ni	8.17	7.01
Cr	10.25	8.33
Al	35.80	44.25
O	32.46	29.74
Y	00	00

500 hrs

Table 3. EDX Analysis at points

Point (Wt%)→ Elements ↓	Overall	Averages of three points
Co	6.45	8.06
Ni	5.18	5.38
Cr	2.77	2.67
Al	49.18	47.32
O	36.43	36.56
Y	00	00

1000 hrs

CGDS He

Fig. 15 EDX analysis of the CGDS coating sprayed with He gas after the oxidation at 900 °C for different times

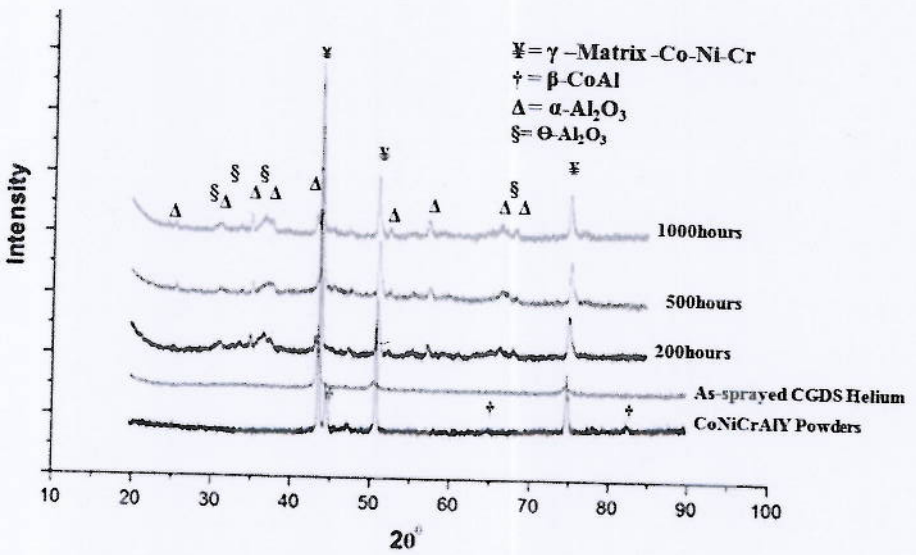

Fig. 16 XRD patterns of oxidized CGDS coating sprayed with He gas at the temperature of 900 °C for different times

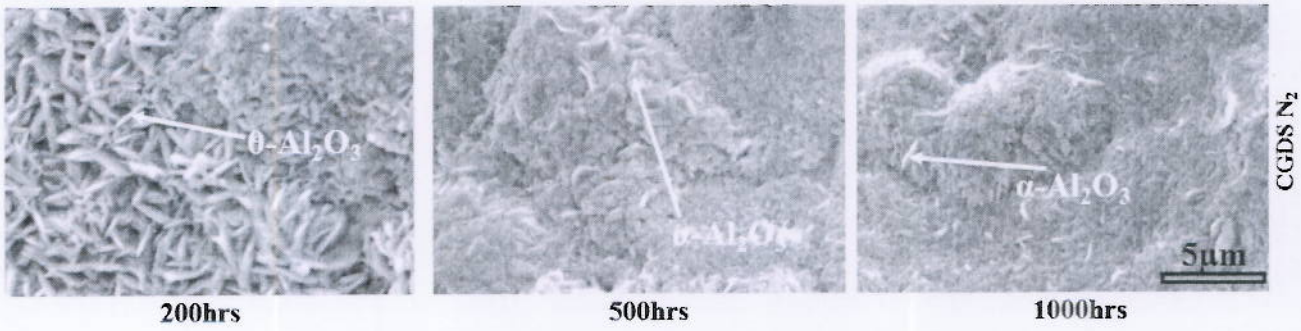

Fig. 17 Surface morphology of the CGDS coating sprayed with N_2 gas after the oxidation at 900 °C for different times

Fig. 18 XRD patterns of oxidized CGDS coating sprayed with N_2 gas at the temperature of 900 °C for different times

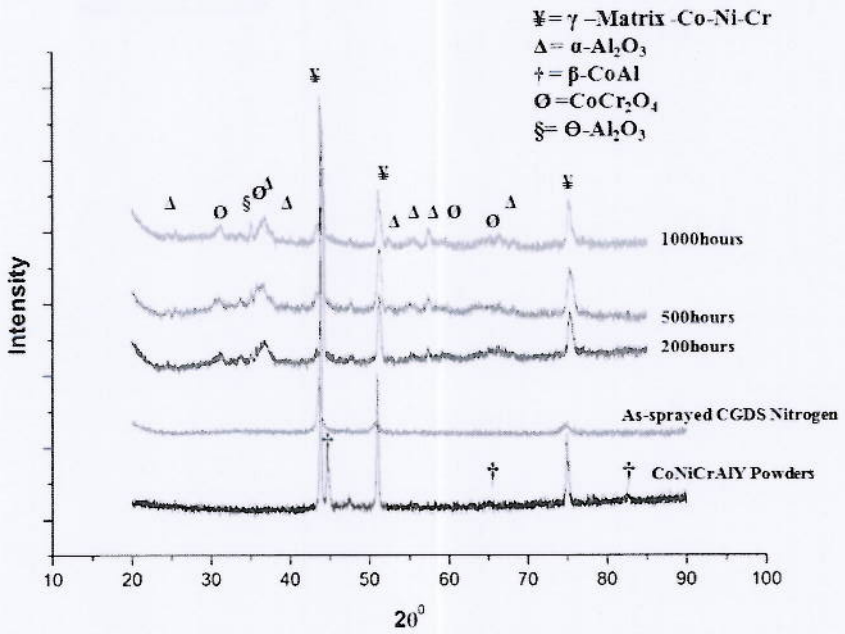

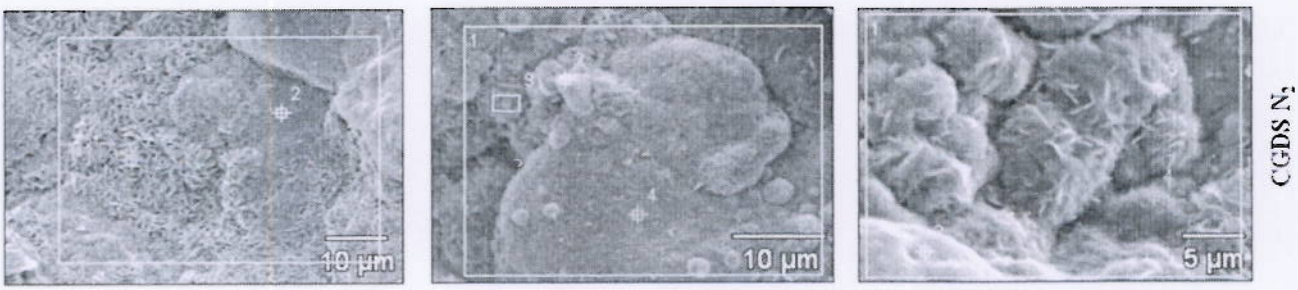

(a) Surface morphology (b) Surface morphology (c) Surface morphology

Table 1. EDX Analysis at point

Point (Wt%) → Elements ↓	Overall	Averages of two points
Co	0.46	1.13
Ni	1.79	1.32
Cr	00	1.21
Al	52.84	54.16
O	44.92	42.16
Y	00	00

200 hrs

Table 2. EDX Analysis at point

Point (Wt%) → Elements ↓	Overall	Averages of three points
Co	4.33	3.57
Ni	1.59	1.00
Cr	4.22	3.75
Al	53.15	46.64
O	36.71	45.03
Y	00	00

500 hrs

Table 3. EDX Analysis at point

Point (Wt%) → Elements ↓	Overall	Averages of three points
Co	6.06	6.36
Ni	4.11	4.02
Cr	2.93	2.61
Al	50.89	47.32
O	36.01	39.67
Y	00	00

1000 hrs

Fig. 19 EDX analysis of the CGDS coating sprayed with N_2 gas after the oxidation at 900 °C for different times

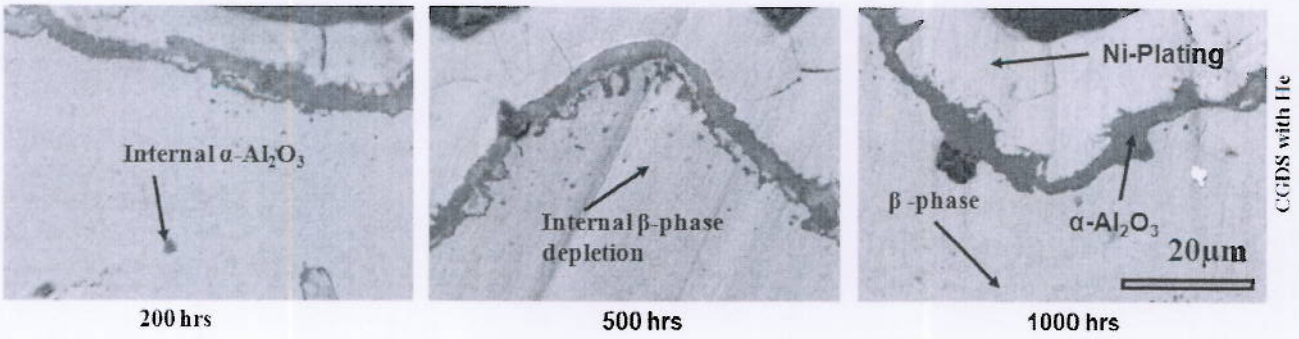

Fig. 20 Cross-section microstructure of the CGDS coating sprayed with He gas after the oxidation at 900 °C for different times

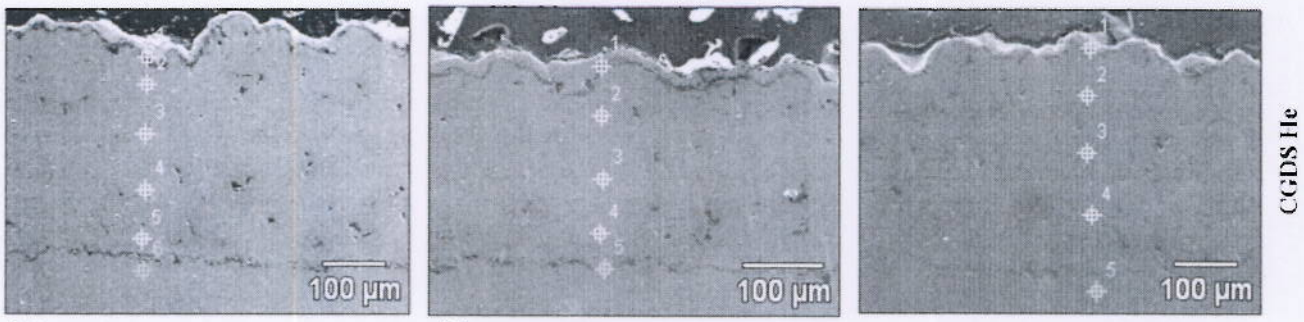

Table 1. EDX Analysis at point

Point (Wt %)→ Elements ↓	1	2	3
Co	3.44	39.90	22.76
Ni	7.39	29.39	47.37
Cr	0.85	23.54	7.07
Al	49.18	7.17	22.79
O	39.13	00	00
Y	00	00	00
Point (Wt %)→ Elements ↓	4	5	6
Co	43.89	24.79	21.71
Ni	26.75	43.65	32.17
Cr	25.36	9.71	45.50
Al	4.00	21.85	0.62
O	00	00	00
Y	00	00	00

200 hrs

Table 2. EDX Analysis at point

Point (Wt %)→ Elements ↓	1	2	3
Co	11.04	34.15	42.67
Ni	8.09	36.94	29.22
Cr	9.88	17.49	24.44
Al	43.53	11.42	3.67
O	27.45	00	00
Y	00	00	00
Point (Wt %)→ Elements ↓	4	5	6
Co	23.52	33.24	
Ni	49.70	32.95	
Cr	7.12	32.30	
Al	19.66	1.50	
O	00	00	
Y	00	00	

500 hrs

Table 3. EDX Analysis at point

Point (Wt %)→ Elements ↓	1	2	3
Co	1.38	34.02	32.04
Ni	1.45	38.21	39.33
Cr	1.18	15.36	14.92
Al	51.12	11.90	13.24
O	44.87	0.51	0.47
Y	00	00	00
Point (Wt %)→ Elements ↓	4	5	6
Co	42.89	20.08	
Ni	27.39	31.88	
Cr	25.73	47.41	
Al	3.83	0.63	
O	0.16	00	
Y	00	00	

1000 hrs

CGDS He

Fig. 21 EDX analysis of cross-section of the CGDS sprayed with He coating after the oxidation at 900 °C for different times

oxidation. It can be seen that the surface is fully covered with an oxide scale composed of Al and O_2 having an acicular morphology. θ-Al_2O_3 usually grows in a needle-like (or whisker-like, blade-like) morphology, while α-Al_2O_3 usually grows in a dense equiaxed structure [11, 13, 16]. This fact means that θ-Al_2O_3 oxide is preferably nucleated during oxidation of the CGDS coating at 200 h at early oxidation stage. Figure 15 shows the EDX analysis with the coating surface layer rich in Al and O. It is reasonable by taking into account XRD result shown in Fig. 16. Coating reveals the existence of θ-Al_2O_3, α-Al_2O_3 and γ-solid solution. A similar observation for CGDS sprayed CoNiCrAlY coatings oxidized at 1,000 °C for up to 100 h is reported by P. Richer et al. [11]. XRD analysis carried out on the Feedstock powder was composed of γ and β-phases as depicted in Fig. 1. Figure 16 shows XRD results for the oxides formed at various stages of oxidation. It is observed that the as-sprayed coating do not retain the typical two-phase microstructure (γ-matrix Co–Ni–Cr solid solution and β-NiAl/CoAl precipitates) initially found in the feedstock powder [14, 16].

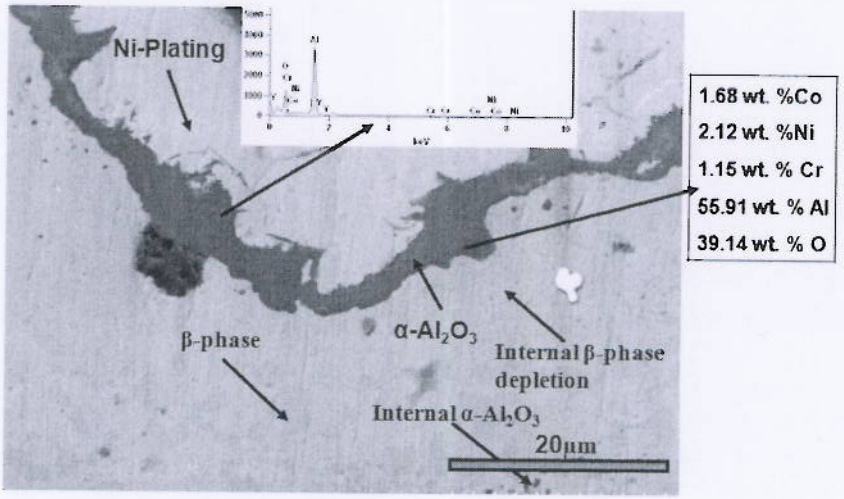

Fig. 22 The TGO layer of the CGDS coating after the oxidation at 900 °C for 1,000 h

The absence of β-phase in as-sprayed coating shows that transformations of microstructure have taken place during deposition. In CGDS coating, the absence of the β-phase is in accordance with findings [11]. CGDS coated samples oxidized at 900 °C for 200, 500 and 1,000 h for isothermal oxidation. During oxidation onset process θ-Al_2O_3 transforms into α-Al_2O_3, it retains its acicular morphology and subsequent growth of α-Alumina appears to be unaffected by the phase transformation [11]. Figure 14 for CGDS coating reveals the existence θ-Alumina as dominant oxide (blade-like crystal) on surface and α-Al_2O_3 is dominant based on peak intensity (Fig. 16). There is no indicating of non alumina forming oxides such as NiO or spinal of Ni, Cr or Al even after 1,000 h of oxidation, indicating the easy availability of aluminum resulting in quick formation of aluminum oxide.

4.9 Characterization of Oxide Scale Morphology, EDX and XRD Analysis of CGDS Coating Sprayed with N_2 Gas Samples Exposed at 900 °C for Different Times

Figure 17 shows the surface morphology of oxidized sample of CGDS sprayed with N_2 coating oxidized at 900 °C for 200, 500 and 1,000 h. Surface morphology at 200 h shows α-Al_2O_3.

It is clear from XRD (Fig. 18) result that the intensity of the peaks associated to $CoCr_2O_4$ spinal-type oxides also increases, while the intensity of the α-Al_2O_3 peaks remains relatively low.

Furthermore form Fig. 19 the EDX analysis shows that the coating surface layer is rich in Al, O are present in the outer oxide layer and small amount of Cr and Co. XRD analyses are carried out on the Feedstock powder is composed of γ and β-phase as depicted in Fig. 1. Figure 18 shows XRD results for the oxides formed at various stages of oxidation. It is observed that the as-sprayed coating do not retain the typical two-phase microstructure (γ-matrix Co–Ni–Cr solid solution and β-NiAl/CoAl precipitates) initially found in the feedstock powder [10, 11]. The absence of β-phase in as-sprayed coating shows that transformations of microstructure have taken place during deposition. In CGDS coating, the absence of the β-phase is in accordance with findings [11].

It is reported to be caused by the dissolution of the β-phase into the γ-matrix due to severe plastic deformation of the particles upon impact [10, 11]. CGDS coating sprayed with N_2 samples oxidized at 900 °C for 200, 500 and 1,000 h for isothermal oxidation. The intensity of the peaks associated to $CoCr_2O_4$ spinal-type oxides also increases, while the intensity of the α-Al_2O_3 peaks remains relatively low. As suggested by Richer, Tang, and Saeidi et al. [10, 13, 16], "spinal" represent either a mixture of some/all of other spinal mixed oxides such as $NiCr_2O_4$, $NiAl_2O_4$, $CoAl_2O_4$, $CoCr_2O_4$ and $NiCo_2O_4$, or a substitutional solid solution of (Ni, Co)(Al, $Cr)_2O_4$. From when θ-Al_2O_3 transforms into α-Al_2O_3, it remains its acicular morphology and subsequent growth of α-Alumina appears to be unaffected by the phase transformation. Coating reveals the existence θ-Alumina as dominant oxide (blade-like crystals) on surface and α-Al_2O_3 is dominant based on peak intensity.

4.10 Cross-Sectional Morphology of Oxidized Scale and EDX Analysis of CGDS Sprayed with He Gas Samples Exposed at 900 °C for Different Times

Figure 20 shows cross-sectional morphology of Oxidized samples. As oxidation time is increased up to 1,000 h for CGDS coating, it is clear from XRD (Fig. 16) that the intensity of the peaks associated to α-Al_2O_3 increases. As oxidation of the coating progresses, aluminum diffuse from

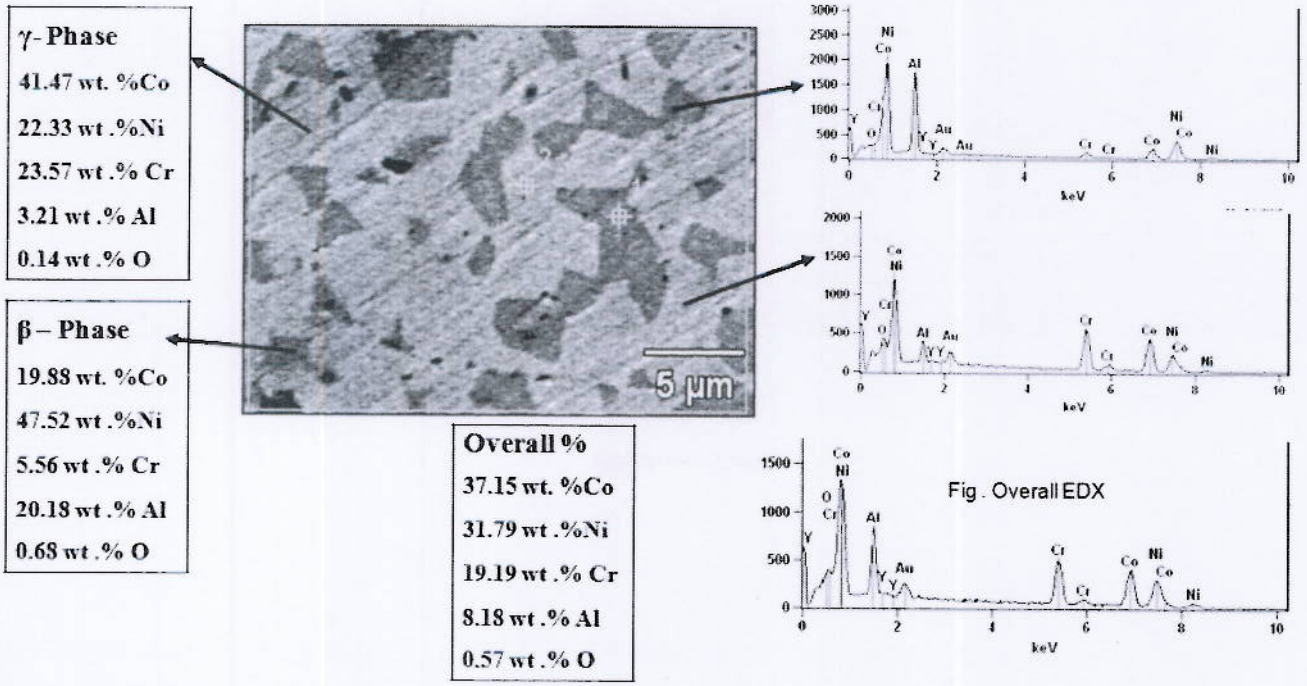

Fig. 23 Microstructure at cross-section of CGDS at 900 °C for 1,000 h

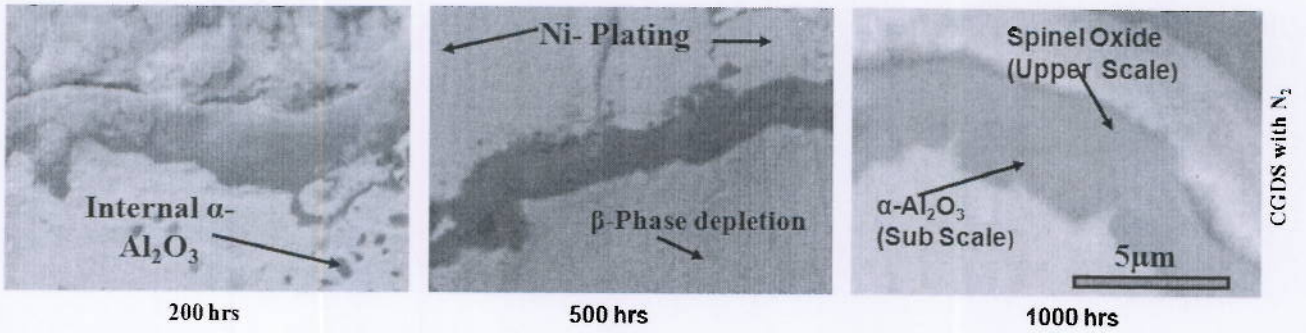

Fig. 24 Cross-section microstructure of the CGDS coating sprayed with N_2 gas after the oxidation at 900 °C for different times

the β-precipitates and reacts to form α-Al_2O_3 scale, thereby resulting in a β-phase depletion zone near the oxidized surface. Even though CGDS coating also included a small amount of pores in the as-sprayed condition, it appears that these pores were not connected to the surface of the coatings possibly. Due to small pores, which allowed oxygen to penetrate and form oxides within the coating. Two phase, namely β-CoAl and γ-CoAl phases, were observed on the coating cross-sections.

After oxidation of 1,000 h, the β-CoAl phase decreased with the increase of oxidation time. During the high temperature exposure, Al diffuses both to the TGO (thermally grow oxide) and to the substrate. The Al concentration in the coating decreases, the β-phase tends to dissolve, often described as an aluminum reservoir, and coating life is often discussed in terms of the depletion of β-phase. After 1,000 h of oxidation for CGDS coating however, the β-phase peaks are no longer discernable by XRD as the β-phase depletion zone has now reached a thickness that is greater than the penetration depth of the incoming X-rays.

Furthermore form (Fig. 21) the EDX point's analysis shown that the point 1 shows rich in Al and O whereas, 2–6 rich in Co, Ni and Cr are detected in the cross-section. EDX spectra and composition of CGDS coating exposed at 900 °C for 1,000 h reported in Fig. 22 showed that the TGO layer is rich in Al and O (Aluminum oxide) [16–18]. Figure 23 shows wt% of β-phase and γ-phase and overall wt at cross-section exposed for 1,000 h at 900 °C of CGDS coating. Comparison of the elemental composition of the both phases, the values presented is an average of five different EDX measurements. The analysis revealed that the darker phase is enriched in Al whereas the brighter phase was enriched in Cr. The γ-phase is the major phase with β regions embedded.

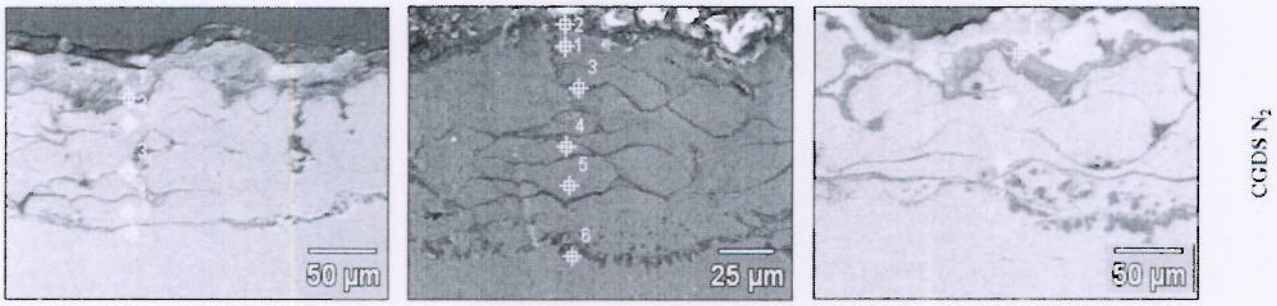

(a) Cross-sectional morphology (b) Cross-sectional morphology (c) Cross-sectional morphology

Table 1. EDX Analysis at point

Point (Wt %)→ Elements ↓	1	2	3	4	5
Co	1.50	39.76	42.05	40.74	27.96
Ni	2.55	35.20	30.79	32..46	33.36
Cr	0.81	22.22	23.05	24.01	38.20
Al	53.49	2.82	4.11	2.80	0.47
O	41.64	00	00	00	00
Y	00	00	00	00	00

200 hrs

Table 2. EDX Analysis at point

Point (Wt %)→ Elements ↓	1	2	3	4	5	6
Co	3.37	41.15	9.45	40.89	40.57	36.03
Ni	5.12	32.70	7.54	33.25	33.17	34.34
Cr	2.37	23.31	7.02	22.21	22.21	28.12
Al	60.16	2.84	46.30	3.49	3.86	0.52
O	28.99	00	29.69	0.17	0.18	1.00
Y	00	00	00	00	00	00

500 hrs

Table 3. EDX Analysis at point

Point (Wt %)→ Elements ↓	1	2	3	4
Co	21.41	42.11	41.21	32.47
Ni	5.97	31.86	31.92	34.22
Cr	21.18	22.62	24.28	32.60
Al	21.74	3.41	2.59	0.71
O	29.69	00	00	00
Y	00	00	00	00

1000 hrs

CGDS N_2

Fig. 25 Cross-section microstructure of the CGDS coating sprayed with N_2 gas after the oxidation at 900 °C for different times

Wt % → Elements ↓	1	2
Co	29.21	3.21
Ni	7.67	6.56
Cr	53.17	5.29
Al	8.95	55.10
O	1.00	29.84
Y	00	00

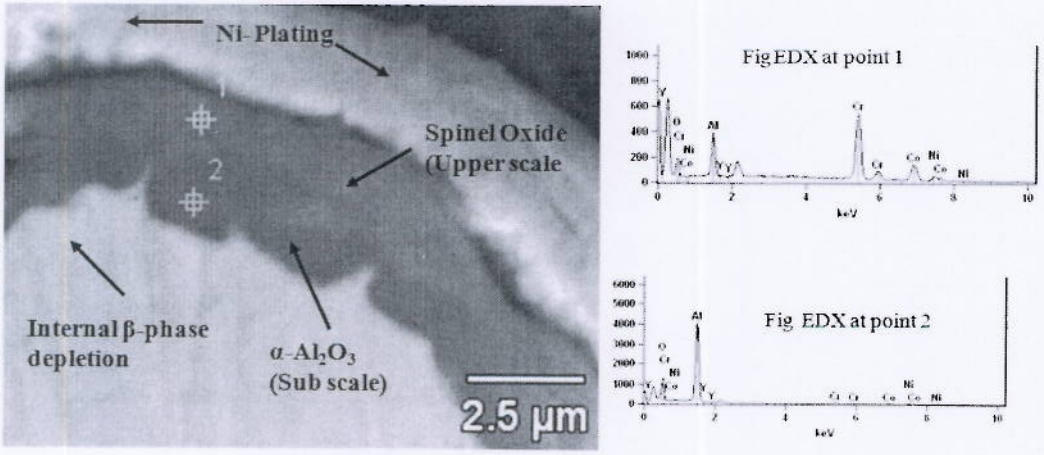

Fig. 26 The TGO Bi-Layered microstructure of the CGDS coating sprayed with N_2 gas after the oxidation at 900 °C for 1,000 h

4.11 Cross-Sectional Morphology of Oxidized Scale and EDX Analysis of CGDS Coating Sprayed with N_2 Gas Samples Exposed at 900 °C for Different Times

Figure 24 shows cross-sectional morphology of oxidized samples. As oxidation time is increased up to 1,000 h for coating, it is clear from XRD (Fig. 19) that the intensity of the peaks associated to $CoCr_2O_4$ spinal-type oxides and α-Al_2O_3 increases. As oxidation of the coating progresses, aluminum diffuses from the β-precipitates and reacts to form α-Al_2O_3 scale, thereby resulting in a β-phase depletion zone near the oxidized surface.

N_2 coating contained many pores, which allowed oxygen to penetrate and form oxides within the coating. CGDS sprayed with N_2 porosity occurred in form of narrow but elongated gaps rather than as spheroidal structures. These gaps were located in between splats and thus impaired the adhesion of the splats. It was noticeable that the discontinuity between the two adjacent powder particles interface in the as-sprayed condition, led to preferred oxidation along the discontinuity boundaries due to the fast oxygen transportation along the discontinuities. After 1,000 h of oxidation for and N_2 coatings however, the β-phase peaks are no longer discernable by XRD as the β-phase depletion zone has now reached a thickness that is greater than the penetration depth

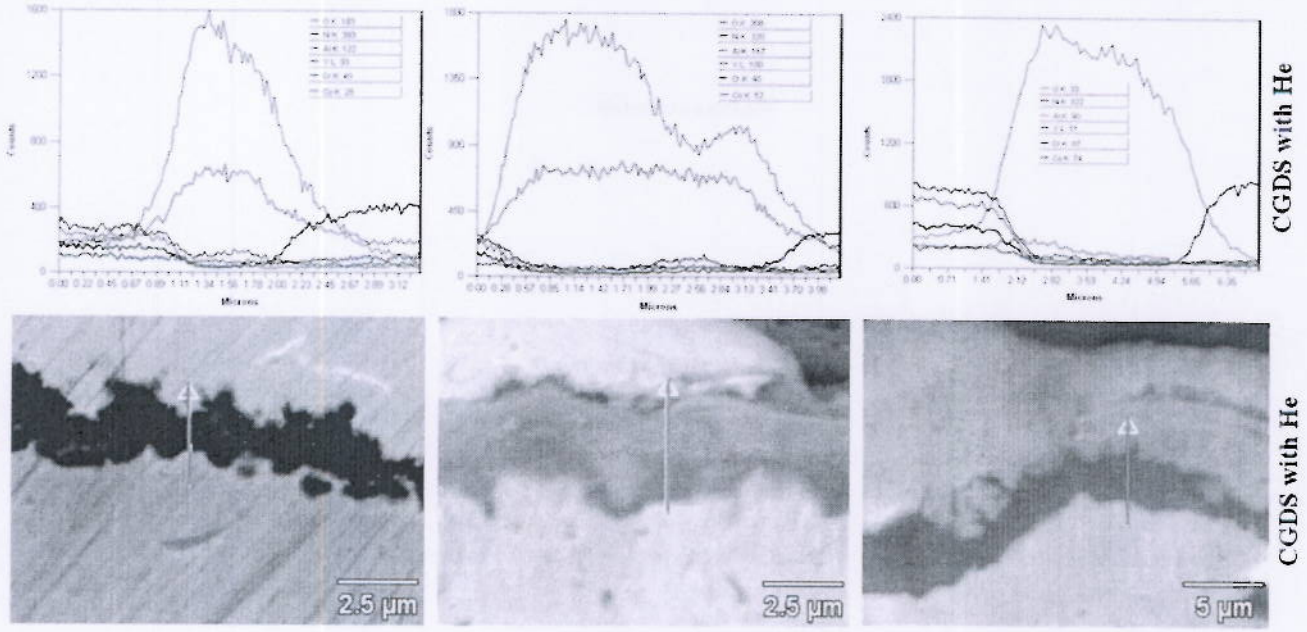

Fig. 27 Variation of elemental composition across the cross-section of CGDS sprayed with He coating after the oxidation at 900 °c for different times and the EDX line-scan along the straight line shown in the BSE image

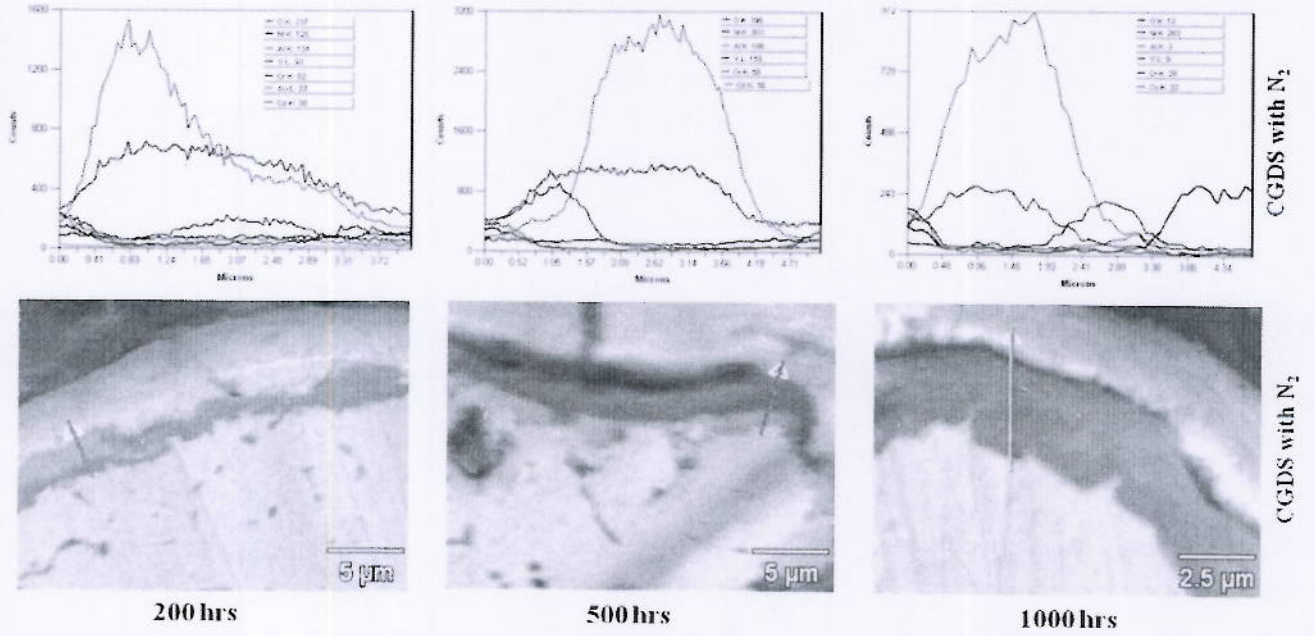

Fig. 28 Variation of elemental composition across the cross-section of CGDS sprayed with N_2 coating after the oxidation at 900 °C for different times and the EDX line-scan along the straight line shown in the BSE image

of the incoming x-rays. Furthermore form (Fig. 25) the EDX point's analysis shows that the point 1 shows rich in Al and O whereas, 2–4 rich in Co, Ni and Cr are detected in the cross-section. EDX spectra and composition of CGDS coating exposed at 900 °C for 1,000 h reported in Fig. 26 showed that the sub scale TGO layer is rich in Al and O (Aluminum oxide), while the upper scale TGO layer contained other metallic oxides (Cr, and Co rich oxides).

4.12 X-Ray Line Scans of CGDS Sprayed with He and N_2 Coatings

X-ray line scans are taken for CGDS sprayed with He and N_2 coating at 900 °C for 200, 500 and 1,000 h. Figure 27 depicted the element distributions along the marked line across the oxide scale obtained by X-ray line scan. X-ray line scans analysis of the CGDS sprayed with He scale

showed Al and O, suggesting the sole formation of alumina whereas CGDS (Fig. 28) with N_2 coating shows an internal layer composed of α-Al_2O_3 and an external scale composed of mixed oxides.

5 Conclusions

1. CoNiCrAlY powder was successfully deposited by the cold-spray technique using He and N_2 as accelerating gases.
2. Cold-spray deposition of CoNiCrAlY powder using helium as carrier gas exhibited dense morphological structure. This effect is attributed to the higher ratio of specific heats and lower mass density of helium as carrier gas.
3. A Bond coat deposited by CGDS sprayed with N_2 gas has higher porosity and several oxide impregnations.
4. Oxidation kinetics of CGDS sprayed with He is an order of magnitude lower than that CGDS coated with N_2. This improvement can be associated partially porosity in CGDS coating, but more due to higher Al concentration on the surface, which resulted in a better selectively an alumina coating.

Acknowledgments The authors wish to thank, ASB Industries, Ohio, USA, for thermal spraying the bond coats samples.

References

1. Balani K, Laha T, Agarwal A, Karthikeyan J, and Munroe N, *Surf Coat Technol* **195** (2005) 272.
2. McCune R C, Papyrin A N, Hall J N, Riggs II W L, and Zajchowski P H, in *Proceedings of 8th National Thermal Spray Conference*, Houston, 11–15 Sept 1995, ASM International, Materials Park, Novelty (1995), p 1.
3. Papyrin A N, Alkimov A P, and Kosarev V F, *United Thermal Spray Conference*, Duesseldorf (1999).
4. Smith M F, Brockmann J E, Dykhuizen R C, Gilmore D L, Neiser R A, and Roemer T J, *Mater Res Soc Symp Proc* **542** (1999) 65.
5. Van Steenkiste T H, Smith J R, Teets R E, Moleski J J, Gorkiewicz D W, Tison R P, Marantz D R, Kowalsky K A, Riggs II W L, Zaichowski P H, Polsner B, McCune R C, and Barnett K J, *Surf Coat Technol* **111** (1999) 62.
6. Van Steenkiste T H, Smith J R, and Teets R E, *Surf Coat Technol* **154** (2002) 237.
7. Lima R S, Karthikeyan J, Kay C M, Lindemann J, and Berndt C C, *Thin Solid Films* **416** (2002) 129.
8. Grujicic M, Saylor J R, Beasley D E, DeRosset W S, and Helfritch D, *Appl Surf Sci* **219** (2003) 211.
9. Gartner F, Borchers C, Stoltenhoff T, Kreys H, and Assadi H, *Adv Sci Appl Technol* **1** (2003) 1.
10. Richer P, Zuniga A, Yandouzi M, and Jodoin B, *Surf Coat Technol* **203** (2008) 364.
11. Richer P, Yandouzi M, Beauvais L, and Jodoin B, *Surf Coat Technol* **204** (2010) 3962.
12. Zhang Q, Li C J, Li Y, Zhang S, Wang X R, Zhang Q, Yang G J, and Li C X, *J Therm Spray Technol* **17** (2008) 838.
13. Tang F, Ajdelsztain L, and Schoenung J M, *Oxid Metals* **61** (2004) 219.
14. Alkimov A P, Kosarev V F et.al., *Sov Phys Dokl* **35** (1990) 1047.
15. Qian L, Li M, Zhou Z, yang H, and Shi X, *Surf Coat Technol* **195** (2005) 264.
16. Saeidi S, Voisey K T, and McCartney D G, *J Therm Spray Technol* **18** (2009) 209.
17. Chen W R, Wu X, Marple B R, Nagy D R, Patnaik P C, *Surf Coat Technol* **202** (2008) 2677.
18. Ajdelsztain L, Picas J A, Kim G E, Bastian F L, Schoenung J, and Provenzano V, *Mater Sci Eng A* **338** (2002) 33.